

Design and analysis of a high temperature superconducting thin film transformer

Le Liang¹ , Yu Wang^{1,2,3} , Zhongming Yan^{1,2} and Weirong Chen¹

¹ School of Electrical Engineering, Southwest Jiaotong University, Chengdu, People's Republic of China

² Key Laboratory of Magnetic Suspension Technology and Maglev Vehicle, Ministry of Education, Southwest Jiaotong University, Chengdu, People's Republic of China

E-mail: wangyu@home.swjtu.edu.cn

Received 21 October 2019, revised 11 February 2020

Accepted for publication 21 February 2020

Published 13 March 2020



Abstract

A novel thin film transformer based on double sided $\text{YBa}_2\text{Cu}_3\text{O}_{7-x}$ (YBCO) thin films with high operating performance, named a high temperature superconducting thin film transformer (HTS-TFT), is proposed and tested. In this paper, we designed and fabricated four different types of HTS-TFT based on double sided YBCO thin film and measured their respective operating parameters (including winding resistance, winding inductance, coupling coefficient, and quality-factor) at liquid nitrogen temperature (LN_2 , 77 K). As the comparative experiment to the HTS-TFT, we also developed the same four types of copper (Cu)-TFT and measured their parameters at both room temperature (RT, 298 K) and LN_2 , to evaluate their behavior. It can be found from the comparative experiments between the HTS-TFTs and Cu-TFTs that the HTS-TFTs (in LN_2) possess better operating parameters than the Cu-TFTs (in LN_2 and RT) and they operate as expected in the power conversion tests. The significance of this work is that the HTS-TFTs can be employed in wireless power transfer systems and other power conversion fields, offering a performance enhancement to power transmission efficiency.

Keywords: high temperature superconducting thin film transformer, power conversion, double sided $\text{YBa}_2\text{Cu}_3\text{O}_{7-x}$ (YBCO) thin film

(Some figures may appear in colour only in the online journal)

1. Introduction

Planar magnetic components, such as planar transformers, can be employed to improve the power density, operating frequency, repeatability, functional integration and low profile of high frequency converters [1–3]. Meanwhile, the cost, size and weight of the planar transformer can also be minimized compared to conventional wire-wound transformers [4–6]. It can be found from [7] that high efficiency can be achieved by employing smaller, thinner and mountable magnetic components. Generally, copper (Cu) is mainly deployed as the winding material of the planar transformer [8–10]. If the surface resistance and current density of the winding material in the operating frequency range can be enhanced, the thickness and size of the planar transformer, as well as the efficiency of the system will be further improved.

High temperature superconducting (HTS) materials, such as tapes, bulks, and thin films, have been applied to almost all electrical and electronic fields (such as transformers, motors, fault current limiters, filters, etc) [11–15]. Due to the zero resistivity and higher current density characteristics of the HTS materials in superconducting states [16], the equipment fabricated with them has better performance than where fabricated with normal conductive materials.

It is known that HTS materials in the superconducting state possess much lower surface resistance compared to normal conductive materials in the frequency range up to GHz level [17, 18]. At the same time, their current density in the superconducting state is also much higher than that of normal conductive materials [16]. Thus it is possible to fabricate the windings of planar transformers using HTS materials.

HTS thin films have been widely used in superconducting electronic fields [15, 19–21]. Meanwhile, they are also deployed as the current limiting and switch devices in

³ Author to whom any correspondence should be addressed.

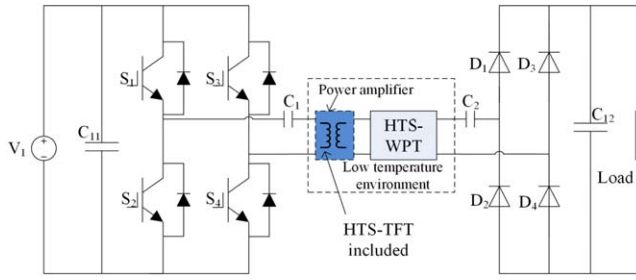


Figure 1. HTS-TFT employed in power amplifier of the HTS-WPT system.

power applications [22–24]. Compared to HTS tapes and bulks, HTS thin films can realize their function by etching the meander-lines in the surface. Thus the compactness and low profile of planar transformers fabricated with HTS thin film can be improved.

In earlier studies, low temperature superconducting thin films have been employed in microwave fields as thin film transformers (TFT) to broaden the band-width [25–27]. Since the emergence of HTS materials, $\text{YBa}_2\text{Cu}_3\text{O}_{7-x}$ (YBCO) single sided thin film has also been utilized as the thin film flux transformer in superconducting quantum interference devices (SQUIDS) to enhance the magnetic field intensity and it is also deployed as the magnetometer and gradiometer flux transformer for SQUIDS [28–30]. However, there is no published literature that has focused on the design, analysis and application of double sided YBCO thin films as the TFT in power converter fields. Due to the structure characteristics of the double sided YBCO thin film, the primary and secondary windings of the HTS-TFT can be fabricated using single sided or double sided thin films, respectively.

With the advent of the all-HTS system and electronic circuit, there is potential for HTS-TFTs to work with other HTS devices. For example, the studies of HTS wireless power transfer systems (HTS-WPTs) have attracted significant attention from researchers in recent years [31–33], and HTS-TFTs have the potential to play the role of power amplifier in HTS-WPTs (as shown in figure 1), to enhance the transmission efficiency of the system. In the HTS application fields that need HTS-TFTs, the cryogenic refrigeration equipment can be shared and the additional costs of refrigeration and operation can be avoided. Furthermore, the efficiency of the cryogenic and operating systems can also be improved compared to adopting conventional planar transformers.

In this paper, a HTS-TFT based on double sided YBCO thin film is proposed and analyzed for the first time. In contrast to the TFT applications of low temperature superconducting thin films in microwave fields and YBCO thin films in SQUID fields, it is the first attempt to design and analyze double sided YBCO thin film based TFTs in applications of power conversion. The parameters of the HTS-TFT in liquid nitrogen temperature (LN_2 , 77 K), including winding resistance, winding inductance, coupling coefficient, and quality-factor (Q-factor), are measured. We also developed the same four types of Cu-TFT and measured their parameters in both LN_2 and room temperature (RT, 298 K) conditions, to

compare the behavior between the HTS-TFT and Cu-TFT. It can be found from the experiment carried out in our laboratory, that the operating performance of the HTS-TFT is better than that of the Cu-TFT. The work in this paper can be conducive to designing HTS-TFTs with higher work efficiency.

The following part of this paper is the operating parameter analysis of the HTS-TFT. Section 3 is the design and fabrication of the HTS-TFT. Section 4 presents the test results of the comparative experiments, to investigate the characteristics comparison between the HTS-TFT and Cu-TFT. At the end of this paper, the experimental results and conclusions are analyzed.

2. Operating parameters analysis of the HTS-TFT

The operating parameter analysis of the proposed HTS-TFT in this paper including the leakage inductance between the primary and secondary windings and the power conversion efficiency [34] are analyzed in the following part.

2.1. Leakage inductance

Although most of the magnetic flux generated by the excitation current can flow along the magnetic path and link the primary and secondary windings via the iron core, some of it is not closed by the iron core (it leaks to the air). This part of the magnetic flux is named the leakage magnetic flux and because of the existence of it, the coupling effect between the primary and secondary windings will be weakened. Some energy is also stored in the leakage inductance, which is given by [35]:

$$E_{lk} = \frac{\mu_0}{2} \sum \int_0^h H^2 \cdot l_w \cdot b_w \cdot dx \quad (1)$$

The symbol h denotes the thickness of the winding layer, l_w and b_w denote the length and width of the winding, respectively. The symbols μ_0 and H denote the vacuum permeability and magnetic field strength, respectively. This part of the energy stored in leakage inductance will lead to voltage spikes and other electromagnetic interference issues, the operating efficiency of the HTS-TFT will also be reduced [35].

Additionally, the leakage inductance would also cause signal attenuation in the operating process and lower the commutation rate of the output terminal [35]. It is obtained as follows:

$$L_{lk} = \mu_0 \cdot \frac{l_w}{b_w} \cdot 4 \left[\frac{h_1 + h_2}{3} + h_0 \right] \quad (2)$$

The symbols h_1 , h_2 , and h_0 denote the thickness of the primary winding, secondary winding, and insulator layer, respectively. The leakage inductance L_{lk} is related to the geometry parameters of the HTS-TFT, thus its undesirable effects can be improved by adjusting the geometry parameters. It can also be represented through the coupling coefficient, as follows:

$$k = \frac{M}{\sqrt{L_1 L_2}} \quad (3)$$

$$M = \frac{L_S - L_D}{4} \quad (4)$$

Where the symbols k and M are the coupling coefficient and mutual inductance between the primary and secondary sides. Symbols L_S and L_D are the inductance of the primary and secondary windings connected in dotted terminals and synonym terminals, respectively. The coupling coefficient in the ideal transformer is 1, but due to the existence of the leakage inductance, its value is not as good as the ideal value. In practical application, the TFT can achieve the better behavior with a higher coupling coefficient.

2.2. Power conversion efficiency

The ideal TFT can deliver energy from the primary side to the secondary side with no energy loss. But, there is inevitable energy losses in the actual TFT, the power conversion efficiency of the TFT should be improved as much as possible. As mentioned in the introduction, the surface resistance of the HTS materials in superconducting state is much smaller than normal conductive materials in the frequency range up to GHz level. Thus the winding Joule losses of the HTS-TFT are much smaller than that of the normal conductive materials based TFT. The power conversion efficiency of the HTS-TFT can be deduced by:

$$\eta = \frac{P_2}{P_1} \times 100\% \quad (5)$$

The symbol η denotes the power conversion efficiency, P_1 is the input power of the primary winding, P_2 is the output power of the secondary winding. P_1 and P_2 can be obtained by:

$$P_1 = \beta S_{2N} \cos \varphi_2 + P_F + P_C \quad (6)$$

$$\begin{aligned} P_2 &= U_2 I_2 \cos \varphi_2 = U_{2N} \frac{I_2}{I_{2N}} I_{2N} \cos \varphi_2 \\ &= \beta U_{2N} I_{2N} \cos \varphi_2 = \beta S_{2N} \cos \varphi_2 \end{aligned} \quad (7)$$

$$\beta = \frac{I_2}{I_{2N}} \times 100\% \quad (8)$$

Where the symbols U_2 , I_2 are the voltage and current of the secondary winding, respectively. Symbols U_{2N} , I_{2N} denote the rated voltage and current of the secondary winding, respectively. The symbols $\cos \varphi_2$ and S_{2N} are the power factor and apparent power of the secondary winding, respectively, symbol β is the load coefficient. P_F is the losses in the iron core, P_C is the Joule losses in winding. By inserting (6), (7) and (8) into (5), η can be simplified as follows:

$$\eta = \frac{\beta S_{2N} \cos \varphi_2}{\beta S_{2N} \cos \varphi_2 + P_F + P_C} \quad (9)$$

It can be seen from (9), that with certain parameters of the TFT, the smaller the winding Joule losses (P_C) are, the higher the efficiency is. Meanwhile, the power conversion efficiency can also be represented by the quality (Q)-factor, as follows:

$$Q = \frac{\omega L_1}{R_1} \quad (10)$$

The symbols L_1 and R_1 are the inductance and resistance of the primary winding, respectively. Symbol ω is the angular frequency of the HTS-TFT. The Q-factor represents the energy losses during delivery from the primary side to the secondary side, and higher Q-factor represents higher power conversion efficiency. We can see from (10) that there exists an inversely-proportional relationship between the Q-factor and R_1 and the Q-factor can be improved by decreasing R_1 . Thus, the power conversion efficiency of the TFT fabricated with HTS material can be improved.

3. Design and fabrication of HTS-TFT

The configuration of the HTS-TFT is shown in figure 2, ferrite (PC 40) is employed as the iron core, and the magnetic circuit is closed with it. The HTS-TFT is fixed on the printed circuit board (PCB) using polyimide and is inserted into the ferrites. The HTS-TFT in this paper is based on double sided YBCO thin film, and the configuration of the thin film is presented in figure 3. The layout structure of the thin film is Au-YBCO-CeO₂-Al₂O₃-CeO₂-YBCO-Au and the layers are symmetrical in reference to the substrate. The diameter and thickness of the substrate is 50.8 mm and 0.5 mm, respectively. The Au layer is the shunt layer to prevent the hot point and oxidation issues of YBCO layer, CeO₂ is the buffer layer to isolate the substrate and YBCO layer. In order to analyze the performance of the HTS-TFT, we have designed four kinds of winding structure, as shown in figure 4. The primary and secondary windings of the HTS-TFT are generated by photoetching and the parameters of the windings are shown in table 1.

As shown in figure 4, the differences between the four kinds of HTS-TFT are the winding type and distribution. In Design 1, the primary winding (L_1) and secondary winding (L_2) of the HTS-TFT are two sided and symmetrical to the substrate of the thin film. In Designs 2, 3 and 4, the windings of the HTS-TFT are in the same side of the thin film. In this paper, the behavior of the HTS-TFTs are investigated through the mentioned four designs. The detailed parameters (winding resistance, winding inductance, coupling coefficient and Q-factor) of the HTS-TFT are measured and analyzed in the following part. The comparison between the HTS-TFT and normal conductive materials (Cu) based TFT (the design parameters of the Cu-TFTs are same as that of the HTS-TFTs, the only difference is that the YBCO layers are replaced with Cu layers) is also analyzed through the experiment carried out in our laboratory.

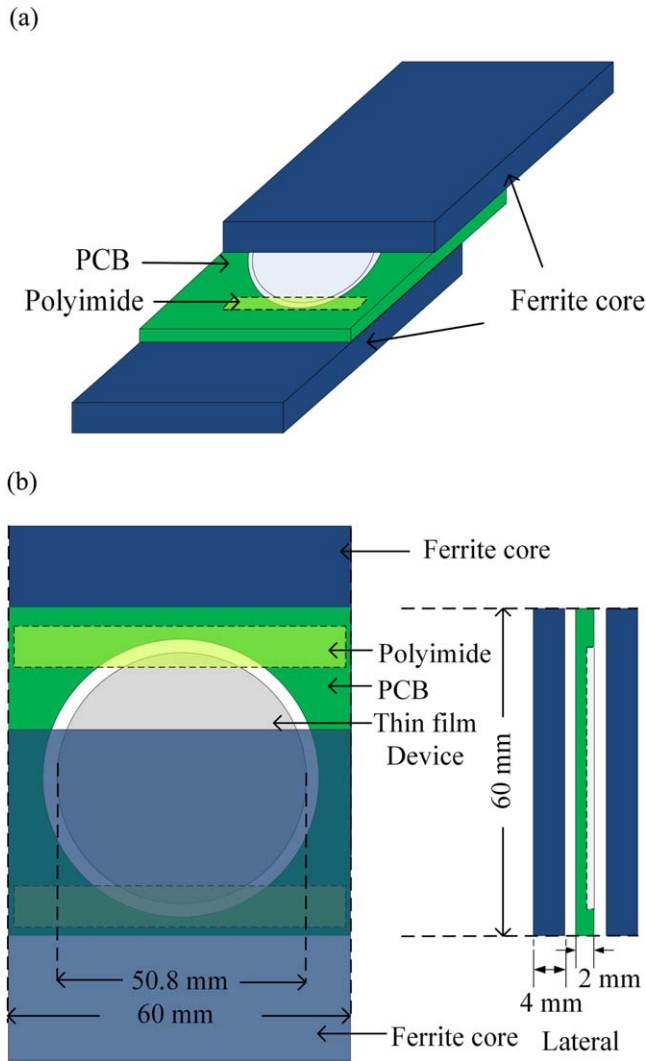


Figure 2. Overview of the HTS-TFT. The ferrite (PC 40) is employed as the iron core to close the magnetic circuit, PCB and polyimide are used to support and fix the HTS-TFT. (a) Three-dimensional view of the HTS-TFT. (b) Geometric parameters of the HTS-TFT.

4. Contrastive experiments and results analysis

As shown in figure 5, the contrastive experiments were carried out in our laboratory to evaluate the behaviors of the HTS-TFTs and Cu-TFTs. An inductance capacitance resistance (LCR) meter is used to measure the operating parameters of the TFT. We measured the parameters of the HTS-TFT in LN₂, as the comparison, the same parameters of the Cu-TFT were also measured in both LN₂ and RT conditions. Because the geometry of the primary and secondary windings are identical, the mentioned parameters were just measured in the primary winding. The operating performance was also analyzed through the contrastive experiments (two-port test network) in the following part.

4.1. Parameters measurement of the HTS-TFT and Cu-TFT

The frequency characteristics of the winding resistance in HTS-TFTs and Cu-TFTs are presented in figure 6. We can see

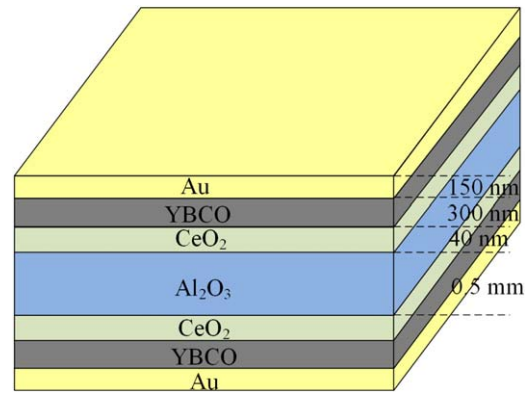


Figure 3. Configuration of the double sided YBCO thin film. Al₂O₃ is the substrate of the thin film, YBCO is the superconducting layer, CeO₂ is the buffer layer, and Au layer is the shunt layer.

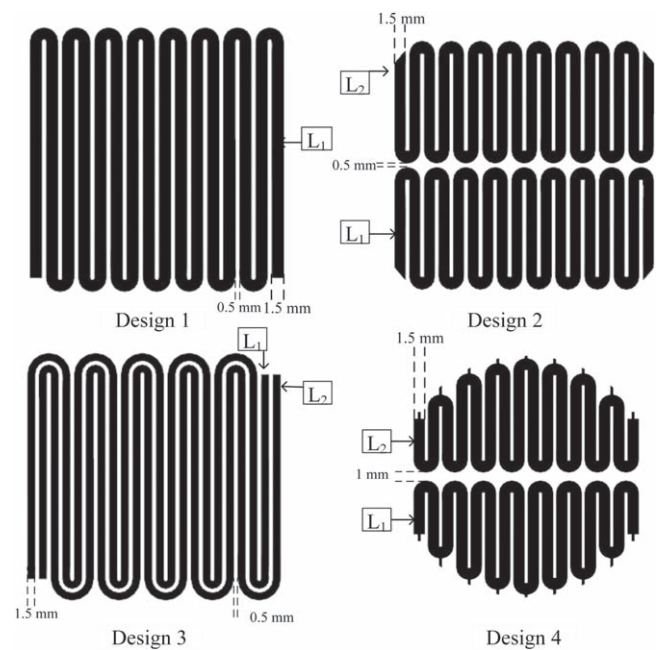


Figure 4. The four different designs of HTS-TFT.

Table 1. Geometric parameters of the HTS-TFT winding.

Group	Parameters of primary and secondary windings
Design 1	1.5 mm-wide, 57 cm-long
Design 2	1.5 mm-wide, 33 cm-long
Design 3	1.5 mm-wide, 37 cm-long
Design 4	1.5 mm-wide, 34 cm-long

from figure 6(a) that all four HTS-TFTs have smaller winding resistances in the measurement frequency range (500 kHz–2 MHz), compared to the same types of Cu-TFTs (at RT). From figure 6(b), the winding resistance of the Cu-TFTs in LN₂ are reduced, but they are still higher than that of the HTS-TFTs. Additionally, the resistance in the HTS-TFTs can be further reduced through improving the machining process of the thin film. Thus the Joule losses in the HTS-TFTs are also much lower than that in the Cu-TFTs.

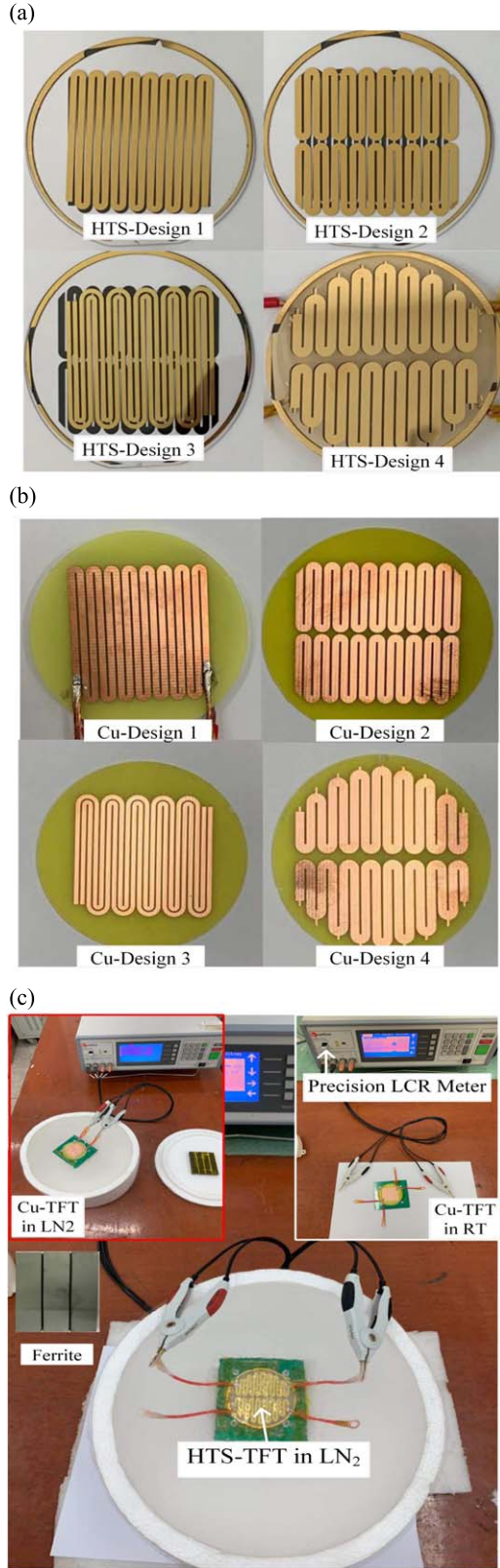


Figure 5. Facilities and overview of the experimental platform. (a) Four different type designs of HTS-TFT. (b) Four different type designs of Cu-TFT. (c) Overview of the experimental measurement platform for HTS-TFT (LN_2) and Cu-TFT (RT and LN_2).

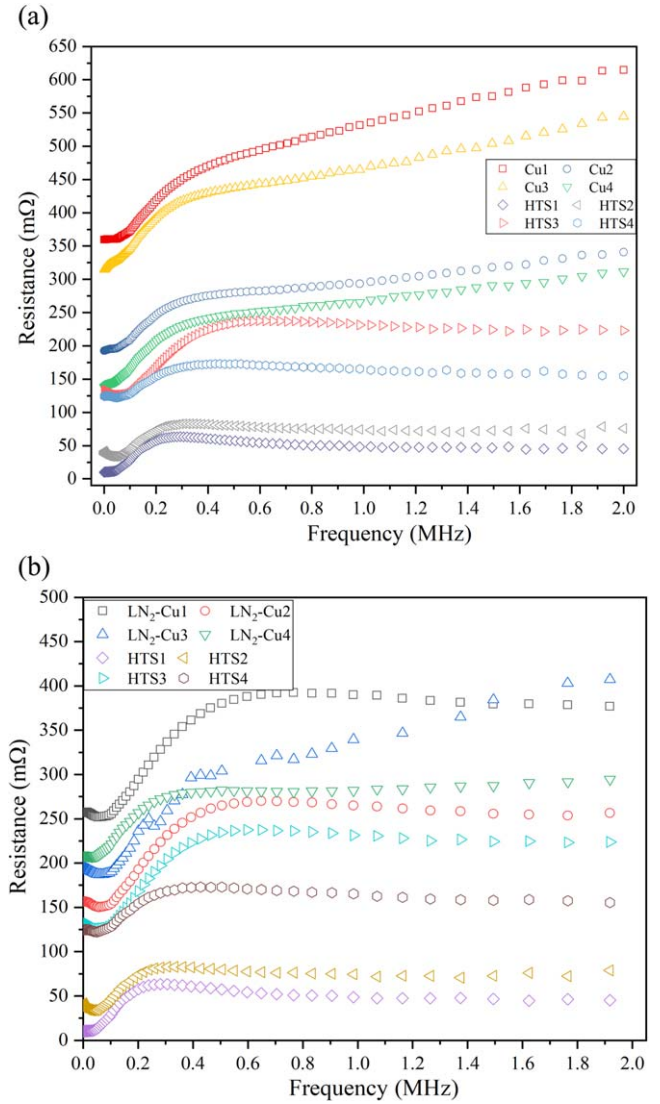


Figure 6. Winding resistance frequency characteristics of the HTS-TFT and Cu-TFT. (a) Winding resistance frequency characteristics of the HTS-TFT (LN_2) and Cu-TFT (RT). Cu_n ($n = 1, 2, 3, 4$) denotes the four designs of the Cu-TFT in RT, and HTS_n ($n = 1, 2, 3, 4$) denotes the four corresponding designs of the HTS-TFT. (b) Winding resistance frequency characteristics of the HTS-TFT (LN_2) and Cu-TFT (LN_2). LN_2 - Cu_n ($n = 1, 2, 3, 4$) denotes the four designs of the Cu-TFT in LN_2 .

The frequency characteristics of the winding inductance in the HTS-TFTs and Cu-TFTs, with and without a core, are presented in figure 7. It can be found from figure 7 that the winding inductance of the HTS-TFTs are increased evidently than that of the Cu-TFTs and the inductance is almost constant during the wider frequency range. The winding inductance of the Cu-TFTs in LN_2 is almost same as its value in RT. Moreover, the core has an obvious effect on the increase of the inductance. The design of the HTS-TFTs can increase the winding inductance effectively.

In addition to increasing the winding inductance of the TFT, the core can also improve the coupling effect between

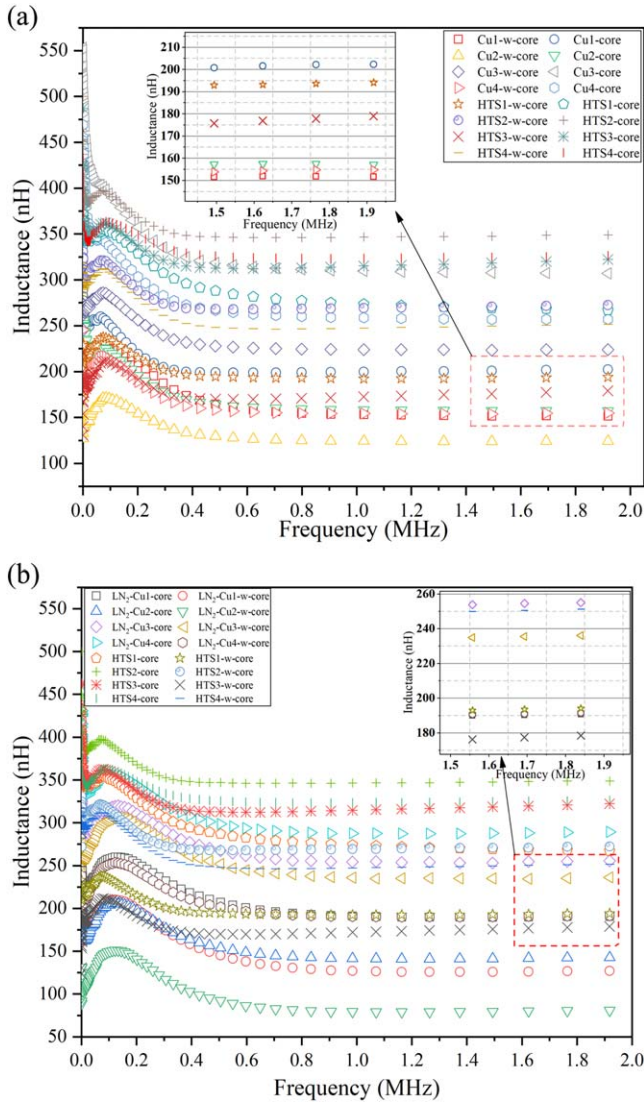


Figure 7. Frequency characteristics of the winding inductance in HTS-TFT and Cu-TFT. (a) Winding inductance measurement of the HTS-TFT (LN_2) and Cu-TFT (RT). $\text{Cu}n\text{-w-core}$ ($n = 1, 2, 3, 4$) denotes the four designs of the Cu-TFT without the core at RT, $\text{Cu}n\text{-core}$ ($n = 1, 2, 3, 4$) denotes the four designs of Cu-TFT with the core at RT, $\text{HTS}n\text{-w-core}$ ($n = 1, 2, 3, 4$) denotes the four designs of HTS-TFT without the core, $\text{HTS}n\text{-core}$ ($n = 1, 2, 3, 4$) denotes the four designs of HTS-TFT with the core. (b) Winding inductance measurement of the HTS-TFT (LN_2) and Cu-TFT (LN_2). $\text{LN}_2\text{-Cu}n\text{-w-core}$ ($n = 1, 2, 3, 4$) denotes the four designs of the Cu-TFT without the core in LN_2 , $\text{LN}_2\text{-Cu}n\text{-core}$ ($n = 1, 2, 3, 4$) denotes the four designs of Cu-TFT with the core in LN_2 , respectively.

the primary winding and secondary winding, in other words, the leakage inductance can also be reduced. According to (4) and (5), the measurement and calculation of the coupling coefficient with and without the core are presented in figure 8. It can be seen from figure 8 that the coupling coefficient in HTS-TFT and Cu-TFT can be improved evidently by adding the core. Design 1 of the HTS-TFT with the core has the best coupling coefficient among the designs. Meanwhile, the coupling coefficient of the Cu-TFT in both RT and LN_2 conditions is almost the same, and it is also not as good as that of the HTS-TFT. Thus the addition of the core is an effective

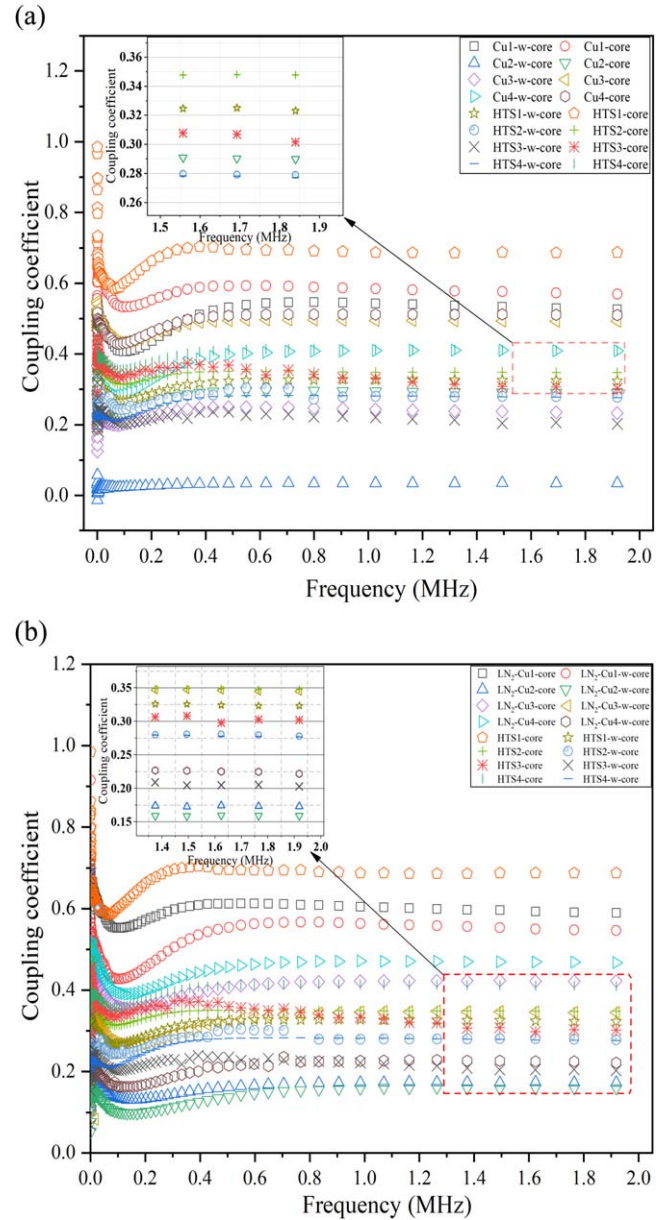


Figure 8. Frequency characteristics of the coupling coefficient between the primary and secondary windings, with and without core. (a) Coupling coefficient of the HTS-TFT (LN_2) and Cu-TFT (RT). (b) Coupling coefficient of the HTS-TFT (LN_2) and Cu-TFT (LN_2).

method to reduce the leakage inductance between the primary and secondary windings of the HTS-TFTs.

As mentioned in section 2, the power conversion efficiency is the vital parameter of a TFT, and it can be reflected by the Q-factor. The frequency characteristics of the Q-factor in HTS-TFTs and Cu-TFTs, with core and without cores, were measured and are presented in figure 9. We find that in both HTS-TFTs and Cu-TFTs, the Q-factor with the core improves apparently compared to the conditions without the core. The Q-factor of the Cu-TFT in LN_2 has a slight increase compared to its value at RT, but the Q-factor of all types of HTS-TFT is higher than the same design of the Cu-TFT, thus, the power conversion efficiency of the HTS-TFT with cores is also higher than the Cu-TFTs.

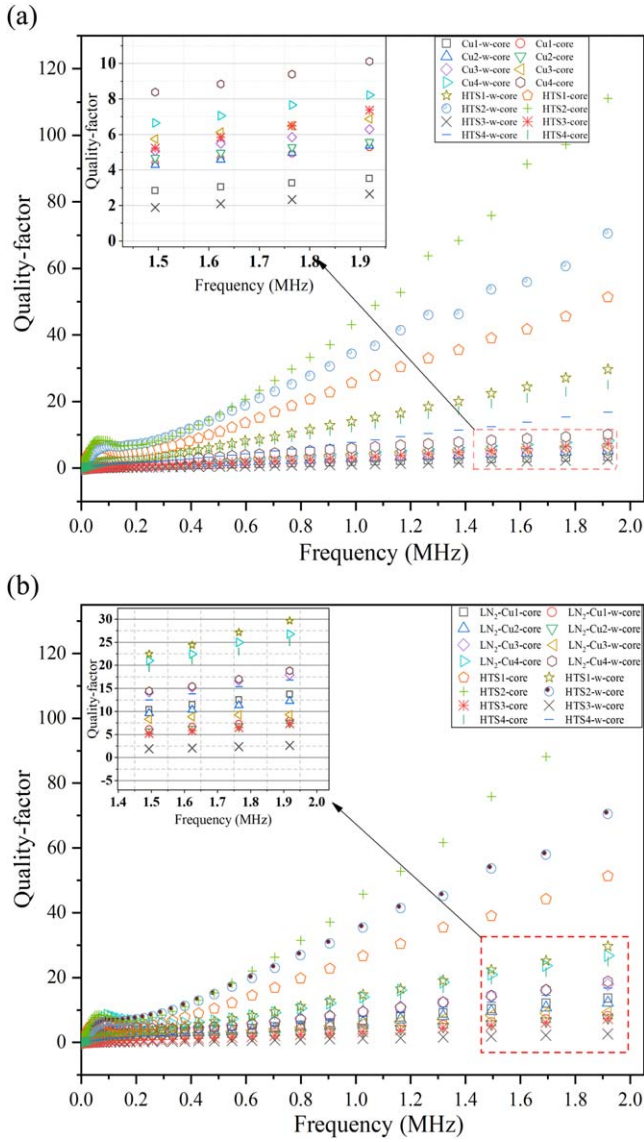


Figure 9. Frequency characteristics of the Q-factor, with and without core. (a) Q-factor of the HTS-TFT (LN₂) and Cu-TFT (RT). (b) Q-factor of the HTS-TFT (LN₂) and Cu-TFT (LN₂).

Table 2. Parameters comparisons of the HTS-TFT with the core.

Parameters	Parameters arrange in ascending order
Winding resistance	HTS1, HTS2, HTS4, HTS3
Winding inductance	HTS1, HTS3, HTS4, HTS2
Coupling coefficient	HTS3, HTS2, HTS4, HTS1
Q-factor	HTS3, HTS4, HTS1, HTS2

To compare the HTS-TFTs and Cu-TFTs, the parameters of each were measured and analyzed (HTS-TFTs are measure in LN₂, Cu-TFTs are measured in both RT and LN₂ conditions). The winding resistance in the four designs of HTS-TFT in superconducting state are much lower than that in the four designs of the Cu-TFT, thus the winding Joule losses in the HTS-TFT are also lower than the Cu-TFTs. Additionally, the designs of the HTS-TFTs show significant improvement in the winding inductance, coupling coefficient and Q-factor,

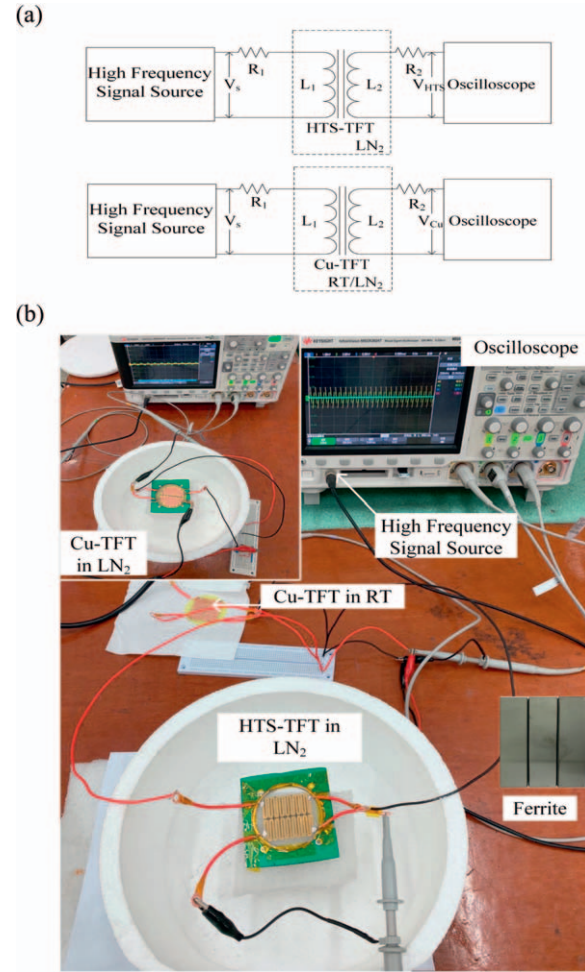


Figure 10. Experimental platform for the operating performance of the HTS-TFT and Cu-TFT. (a) Equivalent electrical circuit. $R_1 = 10 \Omega$, $R_2 = 10 \Omega$, are the sampling resistances. L_1 and L_2 are winding inductance, respectively. (b) Respective test scenarios of the HTS-TFT (LN₂) and Cu-TFT (RT and LN₂).

compared to the Cu-TFT. Meanwhile, the core can improve the winding inductance, coupling coefficient, and Q-factor significantly in the design of the HTS-TFT. Though the parameters of the Cu-TFT in LN₂ are improved compared to their value at RT, its values are not as good as that in HTS-TFTs, and its normal operating ambient is RT, therefore the leakage heat problem in the system can not be avoided. Thus the HTS-TFTs can be better employed in an all-HTS system to improve the operating efficiency. In conclusion, compared to the Cu-TFTs, the operating parameters of the HTS-TFTs show significant improvements and it is possible for HTS-TFTs to be utilized as power converters in power transfer systems to improve their efficiency.

4.2. Operating performance of the HTS-TFT and Cu-TFT

The parameter comparison of the HTS-TFT with the core are presented in table 2. Through comparing the parameters, Design 1 of the HTS-TFT has the lowest winding resistance, highest coupling coefficient and the better Q-factor. We chose it to test the operating behavior of the HTS-TFT.

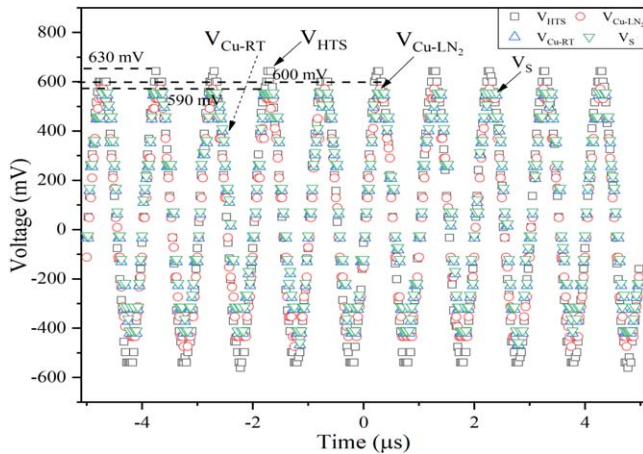


Figure 11. Operating performance of the HTS-TFT and Cu-TFT. V_S is the voltage of the signal source, V_{HTS} is the output voltage of the HTS-TFT, and V_{Cu} is the output voltage of the Cu-TFT at RT, V_{Cu-LN_2} is the output voltage of the Cu-TFT in LN_2 .

To test the operating performance of the HTS-TFT, a small-scale experiment was carried out, and the equivalent electrical circuit, as well as the experimental platform are shown in figure 10. As mentioned, the parameters are almost constant in the wider frequency range, therefore we chose the frequency of the signal source to be 1 MHz. The winding inductances of the HTS-TFT with the core at 1 MHz, are 275 nH and 300 nH respectively. The winding inductances of the Cu-TFT at 1 MHz at RT and LN_2 , are 210 nH and 225 nH, 190 nH and 205 nH, respectively. It can be seen from figure 11 that the terminal voltage of the HTS-TFT is 630 mV and the signal source is 590 mV. It can be found that the voltage conversion ratio of HTS-TFT is more consistent with the winding inductance ratio.

5. Conclusion

In this paper, double sided YBCO thin film based HTS-TFTs to be employed in the power conversion field were proposed and tested for the first time. The thickness and size of the HTS-TFT, as well as the efficiency of the system can be further improved. Four kinds of HTS-TFT were designed to analyze the operating performance of the HTS-TFT. Design 1 of the HTS-TFT has the lowest winding resistance, the highest coupling coefficient and best Q-factor among the four designs. In order to compare the operating parameters, we also designed the same four kinds of Cu-TFT and measured their parameters at both RT and LN_2 conditions. It can be found from the comparative experiments that the parameters of the HTS-TFTs are better than in Cu-TFTs. Through the analysis of operating performance between the HTS-TFTs and Cu-TFTs, the HTS-TFTs can operate as expected. Although some parameters of the Cu-TFTs in LN_2 have a slight increase compared to their values at RT, they are still not as good as the HTS-TFTs. It is effective to illustrate the advantages of the HTS-TFTs in improving the operating efficiency. The parameters of the HTS-TFT can be designed

flexibly, and they can be further increased by improving the material properties and manufacturing process. The application of HTS-TFTs in power converter systems and HTS wireless power transfer systems with different turn ratios should be investigated in future work.

Acknowledgments

This work was supported in part by the National Natural Science Foundation of China under Project U1834203 and in part by the Foundation of the Key Laboratory of Magnetic Suspension Technology and Maglev Vehicles, Ministry of Education, Southwest Jiaotong University, Chengdu, China.

ORCID iDs

Le Liang <https://orcid.org/0000-0001-9738-0852>

Yu Wang <https://orcid.org/0000-0002-5391-8603>

References

- [1] Djuric S M and Stojanovic G M 2014 A compact planar transformer with an improved winding configuration *IEEE Trans. Magn.* **50** 8402204
- [2] Panchal C and Lu J-W 2011 High frequency planar transformer (HFPT) for universal contact-less battery charging platform *IEEE Trans. Magn.* **47** 2764–7
- [3] Han Y, Eberle W and Liu Y-F 2007 A practical copper loss measurement method for the planar transformer in high-frequency switching converters *IEEE Trans. Ind. Electron.* **54** 2276–87
- [4] de Jong E, Ferreira B and Bauer P 2008 Toward next level of PCB usage in power electronic converters *IEEE Trans. Power Electron.* **23** 3151–63
- [5] Djuric S, Stojanovic G, Damnjanovic M and Laboure E 2013 Analysis of the coupling effect in different meander-type winding planar transformers *IEEE Trans. Magn.* **49** 3993–6
- [6] Brucella C, Cecati C and DeMonte F 2008 A coupled electrothermal model for planar transformer temperature distribution computation *IEEE Trans. Ind. Electron.* **55** 3583–90
- [7] Djuric S, Stojanovic G, Damnjanovic M, Radovanovic M and Laboure E 2012 Design, modeling, and analysis of a compact planar transformer *IEEE Trans. Magn.* **48** 4135–8
- [8] Cove S R, Ordonez M, Luchino F and Quaiocoe J E 2013 Applying response surface methodology to small planar transformer winding design *IEEE Trans. Ind. Electron.* **60** 483–93
- [9] Kim D Y, Kim C E and Moon G W 2012 High-efficiency slim adapter with low-profile transformer structure *IEEE Trans. Ind. Electron.* **59** 3445–9
- [10] Zhang J, Ouyang Z, Duffy M C, Andersen M A E and Hurley W G 2014 Leakage inductance calculation for planar transformers with a magnetic shunt *IEEE Trans. Ind. Appl.* **50** 4107–12
- [11] Xin Y *et al* 2012 Development of a 220 kV/300 MVA superconductive fault current limiter *Supercond. Sci. Technol.* **25** 105011
- [12] Liang L, Yan Z, Nie X, Hu Y, Luo K and Wang Y 2019 Experiment of current limiting behavior based on air-core

- superconducting transformer and inductor-capacitor series resonant limiter *IEEE Trans. Appl. Supercond.* **29** 5500204
- [13] Sotelo G G, Sass F, Carrera M, Lopez-Lopez J and Granados X 2018 Proposal of a novel design for linear superconducting motor using 2G tape stacks *IEEE Trans. Ind. Electron.* **65** 7477–84
- [14] Saito T, Kodama S, Saito T, Ohshima S and Saito A 2018 Design of high power handling filter using cascaded quadruplet superconducting bulk resonators *IEEE Trans. Appl. Supercond.* **24** 1500704
- [15] Tan C, Wang Y, Yan Z, Nie X, He Y and Chen W 2019 Superconducting filter based on split-ring resonator structures *IEEE Trans. Appl. Supercond.* **29** 1500404
- [16] Lyatti M, Savenko A and Poppe U 2016 Ultra-thin $\text{YBa}_2\text{Cu}_3\text{O}_{7-x}$ films with high critical current density *Supercond. Sci. Technol.* **29** 065017
- [17] Vendik I 2000 Phenomenological model of the microwave surface impedance of high-Tc superconducting films *Supercond. Sci. Technol.* **13** 974–82
- [18] Mansour R R 2002 Microwave superconductivity *IEEE Trans. Microw. Theory Tech.* **50** 750–9
- [19] Wang Z, Zhang W, Miao W, Liu D, Zhong J-Q and Shi S-C 2018 Electron-Beam evaporated superconducting titanium thin films for antenna-coupled transition edge sensors *IEEE Trans. Appl. Supercond.* **28** 2100204
- [20] Yang X, You L, Zhang L, Lv C, Li H, Liu X, Zhou H and Wang Z 2018 Comparison of superconducting nanowire single-photon detectors made of NbTiN and NbN thin films *IEEE Trans. Appl. Supercond.* **28** 2200106
- [21] Guruswamy T, Goldie D J and Withington S 2014 Quasiparticle generation efficiency in superconducting thin films *Supercond. Sci. Technol.* **27** 055012
- [22] Liang L, Wang Y, Hu Y, Chen W and Yan Z 2019 Protection of electronic circuit based on YBCO superconducting thin film against the induced current interference *IEEE Trans. Appl. Supercond.* **29** 5000606
- [23] Alaraifi S and El Moursi M S 2017 Design considerations of superconducting fault current limiters for power system stability enhancement *IET Gener. Transm. Distrib.* **9** 2155–63
- [24] Tosaka T, Tasaki K, Marukawa K, Kuriyama T, Nakao H, Yamaji M, Kuwano K, Igarashi M, Nemoto K and Terai M 2005 Persistent current magnet cooled by cryocooler (4)—persistent current switch characteristics *IEEE Trans. Appl. Supercond.* **15** 2293–6
- [25] McGinnis D P and Beyer J B 1988 A broad-band microwave superconducting thin-film transformer *IEEE Trans. Microw. Theory Tech.* **36** 1521–5
- [26] Zakosarenko V, Schmelz M, Stolz R, Schönau T, Fritzsche L, Anders S and Meyer H-G 2012 Femtoammeter on the base of SQUID with thin-film flux transformer *Supercond. Sci. Technol.* **25** 095014
- [27] Miklich A H, Przybysz J X and Smith T J 1999 Superconducting thin-film transformers at microwave frequencies *IEEE Trans. Appl. Supercond.* **9** 3062–5
- [28] Wellst F C, Kingston J J, Ferrari M J and Clarke J 1991 Thin-film flux transformers of YBCO *IEEE Trans. Magn.* **27** 2569–72
- [29] Roas B, Fried G, Bar L, Bommel F, Daalmans G and Schultz L 1993 Preparation and characterization of planar YBCO flux transformers *IEEE Trans. Appl. Supercond.* **3** 2422–44
- [30] Shانهsazzadeh F, Jabbari T, Qaderi F and Fardmanesh M 2017 Integrated monolayer planar flux transformer and resonator tank circuit for high-Tc RF-SQUID magnetometer *IEEE Trans. Appl. Supercond.* **27** 1600804
- [31] Chung Y D, Lee C Y, Kim D W, Kang H, Park Y G and Yoon Y S 2017 Conceptual design and operating characteristics of multi-resonance antennas in the wireless power charging system for superconducting maglev train *IEEE Trans. Appl. Supercond.* **27** 3601805
- [32] Zhang G, Yu H, Jing L, Li J, Liu Q and Feng X 2014 Wireless power transfer using high temperature superconducting pancake coils *IEEE Trans. Appl. Supercond.* **24** 4600505
- [33] Yu H, Zhang G, Liu G, Jing L and Liu Q 2018 Asymmetry in wireless power transfer between a superconducting coil and a copper coil *IEEE Trans. Appl. Supercond.* **28** 0600605
- [34] Saket M A, Shafiei N and Ordóñez M 2017 LLC converters with planar transformers: issues and mitigation *IEEE Trans. Power Electron.* **32** 4524–42
- [35] Ouyang Z, Thomsen O C and Andersen M A E 2012 Optimal design and tradeoff analysis of planar transformer in high-power DC–DC converters *IEEE Trans. Ind. Electron.* **59** 2800–10